IEEE Access
Multidisciplinary ⋮ Rapid Review ⋮ Open Access Journal

Received 6 February 2023, accepted 2 March 2023, date of publication 6 March 2023, date of current version 8 June 2023.

Digital Object Identifier 10.1109/ACCESS.2023.3253047

RESEARCH ARTICLE

Harmonics Forecasting of Wind and Solar Hybrid Model Driven by DFIG and PMSG Using ANN and ANFIS

FAWAZ M. AL HADI, HAMED H. ALY, (Senior Member, IEEE), AND TIMOTHY LITTLE
Department of Electrical and Computer Engineering, Dalhousie University, Halifax, NS B3H 4R2, Canada
Corresponding author: Hamed H. Aly (hamed.aly@dal.ca)

ABSTRACT Grid integration of Renewable Energy Systems (RES) involves various types of power electronics-based converters and inverters. The use of these electronic-based devices results in inducing both current and voltage harmonics to the grid. In order to reduce harmonics, especially for large-scale integration of RES, harmonics forecasting is one of many techniques used to design harmonics mitigation devices. The core objective of this work is to develop a novel forecasting model for accurate and reliable harmonics estimation for RES. To achieve this; two hybrid generator models are used. First model consists of wind turbine coupled with Doubly Fed Induction Generator (DFIG) combined with Solar Photo Voltaic (PV) based power generator which are connected to common grid. The second model uses Permanent Magnet Synchronous Generator (PMSG) with wind turbine in conjunction with Solar-PV generator. With real world meteorological data (wind speed and solar irradiation) as inputs, these generators simulate and produce output power with current and voltage waveforms. Harmonics are extracted from these waveforms to record, analyze, arrange and forecast future harmonics. Three parameters namely, Total Harmonics Distortion (THD) and the dominant individual harmonics contents, 11^{th} harmonic (h11) and 13^{th} harmonic (h13) are forecasted for both voltage and current waveforms. Artificial Neural Networks (ANN) and Adaptive Neuro Fuzzy Inference Systems (ANFIS) are the prominent methods used for forecasting. Three types of three-layered ANN structures namely Cascaded Neural Network with Recurrent Local feedback (3LCRNNL), Cascaded Neural Network with Recurrent Global feedback (3LCRNNG) and Cascaded Neural Network with Local and Global feedback (CRNNGL) have been proposed and utilized in this work with hyperbolic tangent as transfer function to adjust weights and scaled conjugate gradient method as optimizer to reduce training error. ANFIS is also employed with subtractive clustering method to improve adaptability and accuracy of forecasts. The results are compared and presented which shows that ANFIS recorded the best performance for THDV and h13 and 3LCRNNGL for h11 for the Wind DFIG-PV model voltage harmonics forecast. For forecasts of the current harmonics, 3LCRNNGL performed best for THDI and h11, whereas ANFIS performed best for h13. For Wind PMSG-PV generator model, ANFIS yields the best results in every scenario involving voltage and current harmonics.

INDEX TERMS Harmonics, renewable energy systems, power quality, artificial neural networks, advanced neuro fuzzy inference system, hybrid models.

I. INTRODUCTION

The generation of electrical energy from renewable energy resources is increasing in these days and that makes it one of the most important topics to deal with. New ideas such as smart grids and microgrids [1] have emerged as a result of the rising penetration of renewable/sustainable energy generation technologies on the Electrical Power System (EPS) [2]. The unpredictable and uncontrollable nature of these RES in terms of power output is one of the fundamental issues

The associate editor coordinating the review of this manuscript and approving it for publication was Dinesh Kumar.

in achieving stability into EPS which result in deteriorating its Power Quality (PQ). Renewable Energy Systems (RES) has different characteristics compared to conventional power sources as they are less controllable, generate undesirable power flow patterns and result in non-sinusoidal current and voltage waveforms. Besides, grid integration of RES involves various types of power electronics-based converters and inverters [2]. These electronic devices at their terminals, produce both current and voltage harmonics, which are transferred to the remainder of the grid [3], [4]. The presence of harmonics could cause overheating of transformers, tripping of circuit breakers, malfunction of protection devices and reduces the life of connected equipment [5], [6]. Therefore, harmonics are one of the most important characteristics that must be kept to a minimum to secure network power quality as per IEEE 519-2014 guidelines [7] and IEC 61000 standards [8], [9], [10]. To quantify the level of distortions contained in the original signal, some indices have been established, such as Total Harmonic Distortion (THD) and Total Demand Distortion (TDD), which are used for voltage and current harmonics [11]. For instance, the voltage THD shall be less than or equivalent to a 5% limit in the Point of Common Coupling (PCC) as per IEEE 519-2014. In order to reduce harmonics, their forecasting is one of many techniques used to design harmonic mitigation devices [12], [13].

II. LITERATURE REVIEW

Traditionally, utility companies used to know the precise industry of the customers who possessed the dominant harmonic sources and consequently the harmonic problems were compensated by employing a passive harmonic filter at the Point of Common Coupling (PCC) of major distorting loads to ensure effectiveness of filters [14], [15], [16]. In recent years, the significant expansion of power electronics-based loads in power systems has fostered substantial distortion in power system signals. Non-linear loads such as power electronics devices (e.g., cycloconverters) and arcing loads (e.g., welding machines and arc furnaces), which are frequently utilized in industry, are the main generators of harmonics in Electrical Power Systems (EPS) [17]. Furthermore, grid integration of renewable energy sources, which involves various types of power electronics-based converters, has recently been found to increase the number of harmonics in the power system [18], [19]. Hence, in order to anticipate and mitigate problems caused by the existence of harmonics, utilities must be able to predict the expected impact of harmonics expected in order to evaluate the compensation required to avoid the consequences due to harmonics. In this regard, efforts have been made by authors to use harmonic estimation to maintain the power quality and ensure harmonic levels under acceptable limits.

Mohan in [20] proposed a harmonics estimation technique based on a Variable Leaky Least Mean Square (VLLMS) algorithm. The proposed method used a leak compensation method to prevent parameter drift. In this procedure, the step size was also adjusted to improve the rate of convergence. A real-time power system was also simulated utilizing various instances, demonstrating the superiority of the proposed method over other systems presented in [20]. In [21], Ivry examined the impact of uncertainty on harmonic prediction in a power system with numerous Voltage Source Converters (VSCs). The Univariate Dimension Reduction (UDR) method was used to forecast the level of harmonic distortion of the VSCs measured at the Point of Common Coupling (PCC) to the grid. In predicting the THD at the PCC, the suggested prediction approach (UDR) ensured full interactions between the harmonic sources (VSCs) and the entire power system. Ray in [22] proposed the concept of adaptive filters that use real time harmonic prediction algorithms by applying Least Mean Square (LMS), Normalised LMS (NLMS) and Recursive Least Square (RLS) methods. This further was used in an active filter to mitigate the time delay produced by the harmonic information acquisition process. Alhaji in [23] and Panoiu et al. in [24] presented a study on the modelling and prediction of total harmonic distortion of current emerging in an electric arc furnace's medium voltage installation. Adaptive Neuro Fuzzy Interference Systems (ANFIS) in MATLAB was used for modelling. The proposed system was able to read 800 data points and forecast THD for another 400 points with a very low error rate.

Rodriguez in [25] introduced a methodology for forecasting of voltage THD for Low Voltage (LV) busbars of residential distribution feeders based on data from a small number of smart meters. Different voltage THD forecasting techniques, namely autoregressive and feed-forward Artificial Neural Networks (ANN) were utilized. This technique allows additional features to be integrated into existing monitoring devices in order to forecast future harmonic distortion. It was demonstrated that a network of advanced smart meters with a minimal number of advanced smart meters is sufficient for accurate harmonic estimations. Furthermore, the research carried out by Mori and Suga et al. [26] proposed a method for predicting power system harmonic voltages based on Artificial Neural Networks (ANN). Harmonic dynamics were handled using Recurrent Neural Networks (RNN). The fifth harmonic voltage was predicted using four RNN's namely Jordan model, Elman model, Noda and Nagao model and the fourth model was proposed in which a network had a context layer between the output and hidden layers as a separate recurrent network. The Elman's approach was found to be more effective than the other models. Kuyunani et al. [27] used the Long Short-term Memory (LSTM) deep learning method. A total of 8103 samples of voltage harmonics measured at the Jeffreys Bay Wind Farm in the Eastern Cape Province were employed in the study to train the network. The suggested model extracted key information from voltage harmonics signals in two steps. Moving window segmentation was used to derive the mean voltage amplitude. The prediction of voltage harmonics generation using LSTM was based on the voltage properties extracted. With a low Root

Mean Square Error (RMSE), the LSTM model forecasted the next 3800 sample mean values.

Žnidarec in his research [28], proposed long-term current harmonic distortion prediction models in order to monitor the effects of current harmonics generated by PV systems. In order to forecast current harmonics, the suggested models use a Multilayer Perceptron Neural Network (MLPNN). The models were trained using data from a year of power quality measurements (1 January–31 December 2018) at the PCC of the 10-kW PV system and the distribution network, as well as meteorological data (solar irradiance and ambient temperature) collected at the test location. In terms of the number of hidden layers and input parameters, six distinct models were constructed, tested, and verified. A three-phase, grid-tied PV plant inverter was used with MLPNN to predict the 5th, 7th, 11th, and 13th. The results of the MLPNN model prediction demonstrated that adding the third input parameter (time of day) to the models improved performance to a small extent.

Hatata and Eladawy [29] used Nonlinear AutoRegressive network with eXogenous inputs (NARX) neural network in their research for predicting the load current harmonics induced into electric power systems. The suggested technology was used on a micro grid at the Khalda – Main Razzak (MRZK) power station in west Egypt, which is a petroleum site. An Electrical Submersible Pump (ESP) that was powered by an induction motor and managed by a Variable Speed Drive (VSD) served as the test nonlinear load. The method for creating the suggested NARX network to simulate nonlinear loads and determine their THD of currents was described in their work. For the purpose of determining the genuine harmonic current of the load and the nonlinearity of each load, the planned network was tested using both simulated pure sinusoidal voltage waveform and standalone measured voltage. By comparing the suggested method with a Recurrent Neural Network (RNN) – based method, it was determined that the suggested NARX method was quicker and more accurate than RNN-based technique.

III. HARMONIC FORECASTING METHODOLOGY

In continuation of the above works, the core objective of this work is to develop a novel forecasting model for accurate and reliable harmonic estimation. ANN [25], [27] and ANFIS [23], [30], [31] are the prominent methods used for forecasting. Three ANN based forecasting models are proposed in this work with different architectures. The ANN also uses hyperbolic tangent as transfer function to adjust weights and scaled conjugate gradient method as optimizer to reduce training error. Moreover, in ANFIS is also employed with subtractive clustering method in effort to improve accuracy. Furthermore, two hybrid generator models are utilized to produce harmonics. The first hybrid model is based on using a Doubly Fed Induction Generator (DFIG) driven via a wind turbine with Photovoltaic panels (Wind DFIG-PV). The other model is the hybrid of wind and Photovoltaic using Permanent Magnet Synchronous Generator (PMSG). The purpose is to generate output waveforms for current and voltages which could represent real world scenario. After getting output waveforms, harmonics are extracted from the data which forms datasets for training and predicting harmonics by using proposed ANN and ANFIS forecasting models.

IV. GENERATOR MODELS

A. HYBRID WIND DFIG-PV MODEL

In order to generate harmonics depicting the real-world response for the wind speeds and solar irradiance inputs, the hybrid Wind DFIG-PV model was introduced. It was created by modifying the DFIG model in the MATLAB library [31], [32] and combining it with PV model. The hybrid wind-DFIG PV Model contains 1.5 MW wind turbines using a wound rotor DFIG coupled with an AC/DC/AC IGBT-based PWM converter. In this model, the wind speed signal is being generated by a signal generator block. Furthermore, the hybrid model also consists of a 1.5 MW rated PV array containing 518 parallel strings. Each string has 7 SunPower SPR-415E modules connected in series. The input irradiance and temperature to PV model is generated from signal generator block. Hence, the hybrid wind DFIG-PV model is constructed for a 3 MW capacity.

The values for wind speeds, solar irradiance and temperature are considered as actual data recorded for Halifax, NS, Canada between 1st June to 24th June 2015. The data is taken form European Commission, Joint Research Centre (JRC) [32]. The grid is modelled as a typical distribution grid. As the inputs are supplied to the model, it was simulated for 19 working days from 1st to 24th, June 2015. All days considered are working days.

B. HYBRID WIND PMSG-PV MODEL

Similar to the Wind-DFIG PV model, the hybrid PMSG-PV model was created by modifying the PMSG model [33], [34] and combining it with PV model. The model contains 1.5 MW wind turbines directly coupled with a multipole PMSG without a gearbox.

C. SIMULATION OF GENERATOR MODELS

The generator models include detailed representation of power electronic IGBT converters. To store and use data for further analysis, the overall data portraying the variations in wind and solar parameters over 19 working days between 1st to 24th June 2015 was split into datasets and the simulation was done in parts. Due to small time step used the period of 19 days seems sufficient to generate forecast. Fig. 1 presents the datasets used:

To log data into the workspace, scope was used. Data was stored in format structure with time to further analyze. A sample of the 3-phase voltage and current waveforms are shown in Fig. 2 and 3 for the time period starting from 5 seconds to demonstrate and visualize the presence of harmonics in the waveform generated for Wind-DFIG PV model. Fig. 2 and 3 indicate a zoomed snapshot of the whole wave which is actually starting from 0.

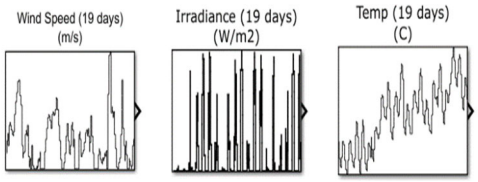

FIGURE 1. Datasets for generator models simulation.

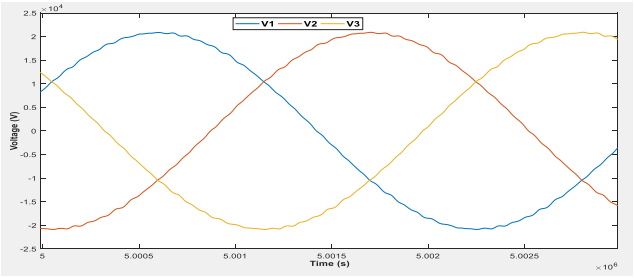

FIGURE 2. Sample voltage waveform (Wind DFIG-PV Model).

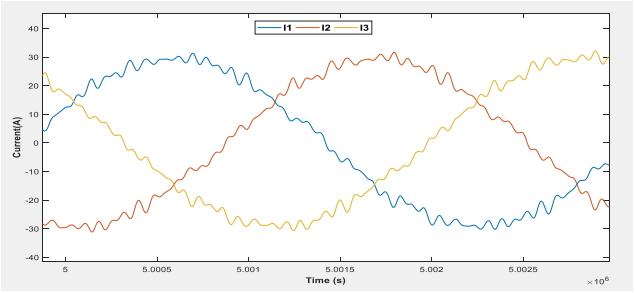

FIGURE 3. Sample current waveform (Wind DFIG-PV Model).

The presence of harmonics can be observed in both current and voltage waveforms. The focus will be kept on the phase 1 voltage and current waveforms to proceed further. All three-phase voltage and current waveforms appear to be the same with 120 degrees out of phase with each other, hence an in-depth analysis and forecasting on one phase is sufficient to realize the overall impact.

In order to extract harmonics, an FFT analysis was carried out on the data procured from scope. The MATLAB command line was used to extract harmonic information. The FFT window employed consist of 5 cycles which extracts the samples from voltage and current waveforms. The FFT samples were extracted for 432 hours (18 days), a total of 4320 samples were recorded with 10 samples logged per hour for both current and voltage waveforms. THD, magnitude of 11^{th} (h11) harmonic component, and magnitude of 13^{th} (h13) harmonic component were extracted from the simulated signals which after statistical analysis were selected as parameters to be forecasted for both voltage and current waveforms:

V. FORECASTING MODELS

A. ARTIFICIAL NEURAL NETWORK (ANN)

McCulloch and Pitts were the first to describe a model of an Artificial Neuron that can mimic the behavior of a biological neuron in [35]. An Artificial Neuron Model in real life executes a sum of products 'n' of inputs denoted by 'p' and weights 'w' connected to them, as well as bias 'b'. To generate the output, this sum is passed into a non-linear transfer function 'f'. The weights 'w' and bias 'b' are variables that can be changed. Fig. 4 shows a model of an Artificial Neuron [36]. Mathematically, n is given by the following equations,

$$n = w_1 p_1 + w_2 p_2 + \ldots + w_R p_R + b \tag{1}$$

$$n = \sum_{j=1}^{R} w_j p_j + b \tag{2}$$

where w_1, $w_2 \ldots w_R$ are weights, p_1, $p_2 \ldots p_R$ are inputs, b is bias and R is number of inputs. The neuron's output is given by

$$a = f\,(n) = f\left(\sum_{j=1}^{R} w_j p_j + b\right) \tag{3}$$

Equation (3) represents the output for basic ANN model consisting of single neuron and single layer. In order to improve the adaptability of ANN, it is constructed with multiple number of neurons and layers called Multi-Layer Perceptron Neural Network (MLPNN). For MLPNN with l number of layers and S^l number of neurons in layer l, (3) can be expressed as follows:

$$a_{lS^l} = f_l\left(n_{lS^l}\right) = f_l\left(\sum_{i=1}^{S^l}\sum_{j=1}^{S^{l-1}} w_{ij} a_{(l-1)j} + b_{lS^l}\right). \tag{4}$$

where l is the number of layers, S denotes the number of neurons, S^l denotes the number of neurons in layer l. There are three MLPNN developed in this work to be used in the hybrid forecast model. They are explained in this section.

1) 3-LAYERED CASCADED NEURAL NETWORK WITH RECURRENT LOCAL FEEDBACK (3LCRNNL)

The 3-Layered Neural Network having cascaded inputs with local feedback is portrayed in Fig. 4. This MPLNN is termed as Three Layered Cascaded Neural Network with Recurrent Local feedback (3LCRNNL). The structure of this network can be observed in Fig. 4 where input is cascaded to each layer and the output from each layer is being fed-back to its input. By designing this structure, the network adaptability is deemed to improve as the network trains with weight adjustments taking into account the feedback and original inputs at each layer of the network. (5) expresses the output of the network.

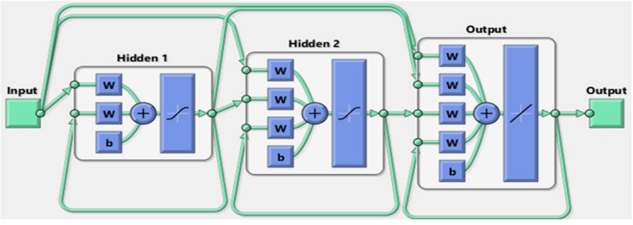

FIGURE 4. Architecture of 3LCRNNL.

2) 3-LAYERED CASCADED NEURAL NETWORK WITH RECURRENT GLOBAL FEEDBACK (3LCRNNG)

The second MPLNN combines the Cascaded Neural Network with Recurrent Network with Global feedback to create Cascaded Neural Network with Recurrent Global feedback (3LCRNNG). Fig. 5 shows its construction and (6) presents its output equation. With the feedback from output layer to input layer and original inputs cascaded to each successive layer separately, effort is being made to create a strong correlation between input and output in order for the network to produce accurate forecast.

$$
\begin{aligned}
\boldsymbol{a}_{3s^3} &= \boldsymbol{f}_3\left(\boldsymbol{n}_{3s^3}\right) = \boldsymbol{f}_3\left(\sum_{i=1}^{s^3}\sum_{j=1}^{R}\boldsymbol{w}_{ij}\boldsymbol{p}_j\right.\\
&\quad + \sum_{i=1}^{s^3}\sum_{j=1}^{s^1}\boldsymbol{w}_{ij}\boldsymbol{f}_1\left(\sum_{i=1}^{s^1}\sum_{j=1}^{R}\boldsymbol{w}_{ij}\boldsymbol{p}_j\right.\\
&\quad + \sum_{i=1}^{s^1}\sum_{j=1}^{s^1}\boldsymbol{w}_{ij}\boldsymbol{a}_{1j}(t-1) + \sum_{i=1}^{s^1}\sum_{j=1}^{s^3}\boldsymbol{w}_{ij}\boldsymbol{a}_{3j}(t-1)\\
&\quad \left. q + \boldsymbol{b}_{1s^1}\right)\\
&\quad + \sum_{i=1}^{s^3}\sum_{j=1}^{s^2}\boldsymbol{w}_{ij}\boldsymbol{f}_2\left(\sum_{i=1}^{s^2}\sum_{j=1}^{R}\boldsymbol{w}_{ij}\boldsymbol{p}_j + \sum_{i=1}^{s^2}\sum_{j=1}^{s^1}\boldsymbol{w}_{ij}\boldsymbol{a}_{2j}\right.\\
&\quad + \sum_{i=1}^{s^2}\sum_{j=1}^{s^2}\boldsymbol{w}_{ij}\boldsymbol{a}_{2j}(t-1) + \sum_{i=1}^{s^2}\sum_{j=1}^{s^3}\boldsymbol{w}_{ij}\boldsymbol{a}_{3j}(t-1)\\
&\quad \left.\left. + \boldsymbol{b}_{2s^2}\right) + \sum_{i=1}^{s^3}\sum_{j=1}^{s^3}\boldsymbol{w}_{ij}\boldsymbol{a}_{3j}(t-1) + \boldsymbol{b}_{3s^3}\right) \qquad (5)
\end{aligned}
$$

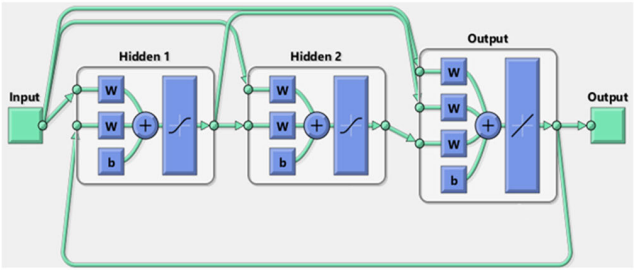

FIGURE 5. Architecture of 3LCRNNG.

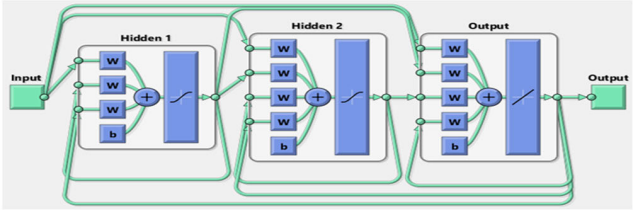

FIGURE 6. Architecture of 3LCRNNGL.

$$
\begin{aligned}
\boldsymbol{a}_{3s^3} &= \boldsymbol{f}_3\left(\boldsymbol{n}_{3s^3}\right) = \boldsymbol{f}_3\left(\sum_{i=1}^{s^3}\sum_{j=1}^{R}\boldsymbol{w}_{ij}\boldsymbol{p}_j\right.\\
&\quad q + \sum_{i=1}^{s^3}\sum_{j=1}^{s^1}\boldsymbol{w}_{ij}\boldsymbol{f}_1\left(\sum_{i=1}^{s^1}\sum_{j=1}^{R}\boldsymbol{w}_{ij}\boldsymbol{p}_j\right.\\
&\quad + \sum_{i=1}^{s^1}\sum_{j=1}^{s^2}\boldsymbol{w}_{ij}\boldsymbol{a}_{1j}(t-1) + \boldsymbol{b}_{1s^1}\Big)\\
&\quad + \sum_{i=1}^{s^3}\sum_{j=1}^{s^2}\boldsymbol{w}_{ij}\boldsymbol{f}_2\left(\sum_{i=1}^{s^2}\sum_{j=1}^{R}\boldsymbol{w}_{ij}\boldsymbol{p}_j + \sum_{i=1}^{s^2}\sum_{j=1}^{s^1}\boldsymbol{w}_{ij}\boldsymbol{a}_{1j}\right.\\
&\quad + \sum_{i=1}^{s^2}\sum_{j=1}^{s^2}\boldsymbol{w}_{ij}\boldsymbol{a}_{2j}(t-1) + \boldsymbol{b}_{2s^2}\Big)\\
&\quad \left. + \sum_{i=1}^{s^3}\sum_{j=1}^{s^3}\boldsymbol{w}_{ij}\boldsymbol{a}_{3j}(t-1) + \boldsymbol{b}_{3s^3}\right) \qquad (6)
\end{aligned}
$$

$$
\begin{aligned}
\boldsymbol{a}_{3s^3} &= \boldsymbol{f}_3\left(\boldsymbol{n}_{3s^3}\right) = \boldsymbol{f}_3\left(\sum_{i=1}^{s^3}\sum_{j=1}^{R}\boldsymbol{w}_{ij}\boldsymbol{p}_j\right.\\
&\quad + \sum_{i=1}^{s^3}\sum_{j=1}^{s^1}\boldsymbol{w}_{ij}\boldsymbol{f}_1\left(\sum_{i=1}^{s^1}\sum_{j=1}^{R}\boldsymbol{w}_{ij}\boldsymbol{p}_j\right.\\
&\quad + \sum_{i=1}^{s^1}\sum_{j=1}^{s^3}\boldsymbol{w}_{ij}\boldsymbol{a}_{2j}(t-1) + \boldsymbol{b}_{1s^1}\Big)\\
&\quad + \sum_{i=1}^{s^3}\sum_{j=1}^{s^2}\boldsymbol{w}_{ij}\boldsymbol{f}_2\left(\sum_{i=1}^{s^2}\sum_{j=1}^{R}\boldsymbol{w}_{ij}\boldsymbol{p}_j\right.\\
&\quad \left.\left. + \sum_{i=1}^{s^2}\sum_{j=1}^{s^1}\boldsymbol{w}_{ij}\boldsymbol{a}_{2j} + \boldsymbol{b}_{2s^2}\right) + \boldsymbol{b}_{3s^3}\right) \qquad (7)
\end{aligned}
$$

3) 3-LAYERED CASCADED NEURAL NETWORK WITH RECURRENT GLOBAL FEEDBACK (3LCRNNG)

As the name suggests, in order to integrate the networks to improve accuracy, in the third MPLNN, the inputs are cascaded to the next layers and each layer also receives feedback from its output as well as from the output layer. Fig. 6 below shows the architecture and (7) depicts the output of 3-Layered Cascaded Neural Network with Recurrent Local & Global feedback (3LCRNNGL). From fig. 6, it can be observed that the architecture of this network considers feedback from output layer to each hidden layer and also connects the feedback of each hidden layer to its own input. The original input is also cascaded to each layer separately. This is an effort to increase the adaptability of the network so as to train and adjust weights in order to produce accurate forecast.

4) ANN ARCHITECTURE

The ANN models used in this work are aimed to predict the next step harmonics. The ANN uses previously observed

harmonic patterns of simulated data for training and learning in order to provide forecasts. Furthermore, for the ANN to work well, there must be a strong correlation between the inputs and outputs. Additionally, in order to improve performance, the hidden layer and output layer weights must be carefully adjusted throughout the training phase. Hence, determining the architecture specifically, the ideal number of hidden layers, the number of neurons in each layer, and the role of each layer's activation becomes essential for better performance. To improve weight adjustment, the hyperbolic tangent transfer function was used for the hidden layers. By default, MATLAB uses sigmoid transfer function. For a complex and non-linear dataset, the selection of hyperbolic transfer function is more beneficial as compared to the sigmoid function and establishes two features that differentiate hyperbolic tangent function with sigmoid function.

1. The sigmoid function has a substantially smaller slope than the hyperbolic tangent function.

2. The sigmoid function always responds positively, but the hyperbolic tangent function responds negatively for negative input values and positively for positive input values.

The larger slope of the hyperbolic tangent function indicates that it responds more strongly to even a modest change in the input variable. As a result, it can provide a considerably more nonlinear response and can better distinguish between subtle variations in the input variable. The 3LCRNNL, 3LCRNNG, and 3LCRNNGL ANN models and architecture used in this paper employ the hyperbolic tangent transfer function in all their hidden layers. Further to increase the resilience of models, linkages between input and output in various combinations are created. Wind Speed, Solar Irradiation One day before observation of predicted parameter and Two days before observation of predicted parameter are used as inputs to train ANN and ANFIS. All the three hybrid ANN models comprise of eight nodes in the first hidden layer and sixteen nodes in the second hidden layer. The number of layers selected are optimized to give the best performance. The optimization was done by trial-and-error method by using different combinations of hidden layers.

Moreover, the ANN models employ scaled conjugate gradient as an optimizer for the reduction of the error function (training). This optimal harmonic prediction optimizer was identified by trial and error. Based on conjugate directions, Moller [37] created the scaled conjugate gradient (SCG) algorithm. Unlike other conjugate gradient algorithms, which need a line search at each iteration, this technique does not do a line search at each iteration. SCG was created to do away with the tiresome line search. A network training function called "trainscg" in MATLAB changes bias and weight variables using the scaled conjugate gradient approach. The quadratic approximation of the error function is used to determine the step size in the SCG algorithm, which further increases its robustness and independence from user-defined parameters [37].

B. ADAPTIVE NEURO FUZZY INFERENCE SYSTEM (ANFIS)

ANFIS was introduced in early 1990s by Jang Roger, who proposed to integrate the ANN and Fuzzy Logic. Based on Takagi–Sugeno Fuzzy Inference System, ANFIS combines ANN's capability of self-learning with Fuzzy System's logical inference ability, robustness and ease in implementing the rules bases. The ANFIS systems are extremely effective and easy to implement specially in cases which face problems of non-linearity and uncertainty in data [38]. A typical fuzzy rule in a Sugeno fuzzy model has the following format:

$$IF\ x\ is\ A\ and\ y\ is\ B, THEN\ z = f(x, y) \tag{8}$$

where A and B are fuzzy sets, z = f (x, y) is a crisp function defining the output. The function f (x, y) is typically a polynomial which describes the output based on the input variables x and y within the fuzzy region specified by the fuzzy sets of the rule. Considering a first order Sugeno FIS which contains two rules:

$$\begin{aligned} &Rule\ 1:\ IF\ x\ is\ A1\ and\ y\ is\ B\ 1, THEN\ f1 \\ &= p1x + q1y + r1 \\ &Rule\ 2:\ IF\ x\ is\ A2\ and\ y\ is\ B\ 2, THEN\ f2 \\ &= p2x + q2y + r2 \end{aligned} \tag{9}$$

The final output is a summation of all incoming signals expressed as follows:

$$f = \sum\nolimits_i \bar{w}_i f_i = \frac{\sum_i \bar{w}_i f_i}{\sum_i \bar{w}_i} \tag{10}$$

In order to model data uncertainty, ANFIS essentially combines the learning capabilities of NNs with those of a FIS. It is simple to train an ANFIS model without the need for detailed subject-matter expertise. ANFIS has the benefit of utilizing both verbal and numerical information. The NN component of the model also enables data classification and pattern recognition. The ANFIS model is more transparent when compared to NN. Thus, the flexibility, nonlinearity, and quick learning of ANFIS are its benefits. However, the system becomes exceedingly challenging to execute practically when the number of inputs to the standard ANFIS system's fuzzy system rises. Additionally, as more inputs and membership functions are selected for each input, the more training time is needed for the standard ANFIS system. Moreover, as the number of membership functions per input increases, so do the fuzzy rules. Using the ANFIS method for prediction, which is based on clustering, makes it simple to overcome the challenges listed above [16].

Subtractive clustering is a quick procedure for figuring out how many clusters there are and where their centers are for making predictions. Moreover, it is also very useful when data characteristics are uncertain to be clustered. The subtractive clustering method is an extension of the mountain clustering method proposed in [39]. This method evaluates each data point as a prospective cluster center candidate and then determines each data point's potential by calculating the density of the data points around it. When it is unclear how many data

distribution centers will be needed, this strategy is used. This is the case in this paper due to which subtractive clustering is used. The approach is iterative, and it assumes that any point could serve as the center of a cluster depending on where it is in relation to other data points. It involves selecting the point with the best likelihood of being the cluster center, then deleting every other point inside the first cluster center's radius (the radius is defined by the neighborhoods of the center). Additionally, to find the next cluster center, recalculate the potential of the other spots. Finally, keep doing this until all the data is contained within a cluster center's radius [40]. For optimization following parameters were changed to improve the performance. Specify the following clustering options:

- Squash factor - Only find clusters that are far from each other.
- Accept ratio - Only accept data points with a strong potential for being cluster canters.
- Reject ratio - Reject data points if they do not have a strong potential for being cluster canters.

VI. IMPLEMENTATION OF FORECASTING MODELS

A. DATA GENERATION FROM GENERATOR MODELS

The two generator models (Wind DFIG-PV and Wind PMSG-PV) were used to implement the proposed forecasting models. Real wind speed and solar irradiation data for Halifax was used as recorded for working days between June 1st and 24th, 2015 [32]. The generator models produce output power, voltage and current waveforms. Harmonics were extracted for voltage and current using FFT to be used as inputs for the forecasting models. There was a total of 19 working days for the simulation period mentioned. The data for the first 18 days was used to train the networks to forecast the 19th day harmonics parameters which were compared with simulated results for the 19th day to check accuracy and calculate error.

B. SELECTION OF INPUTS

The selection of input is crucial to achieve accurate forecast. Inputs shall be carefully selected from the available data by analyzing the trends for the target signal. In this paper, the amplitude of individual harmonic for dominant harmonics and the Total Harmonic Distortion (THD) are the target signals.

C. DATA PRE-PROCESSING

Data pre-processing is a step in which all data points are normalized between values of 0 and 1. This simplifies the calculations and uniformly presents all input parameters under one scale. Equation 11 was used to normalize data:

$$x_{norm} = \frac{x - x_{min}}{x_{max} - x_{min}} \tag{11}$$

where, x_{norm} is the normalised data point, x is the actual data point, x_{min} is the minimum data point in the series and x_{max} is the maximum data point in the series.

D. NETWORK TRAINING

For the execution of training, the data collected from generator models was further separated into training and testing datasets. The major parameters to create these datasets were amplitude of dominant harmonics (h11 and h13), Total Harmonic Distortion and generator model input parameters (wind speed and solar irradiation).

E. EVALUATION OF FORECASTING MODELS

The performance of forecasting models is evaluated based on percentage of Root Mean Squared Error (RMSE%) and Mean Absolute Error percentage (MAE%) indices. The lower the root mean square error (RMSE) means lesser outliers in the output and lower mean absolute error (MAE) means lesser average error of the overall outputs and thus the better a model performance. With time step N, target sequence denoted by t_i while forecast sequence by f_i, i denotes the datapoint, (12) and (13) presents the formulas to calculate the RMSE% and MAE%:

$$RMSE(\%) = \sqrt{\frac{1}{N}\sum_{i=1}^{N}(t_i - f_i)^2} \times 100 \tag{12}$$

$$MAE(\%) = \frac{1}{N}\sum_{i=1}^{N}|t_i - f_i| \times 100 \tag{13}$$

VII. RESULTS

A. HARMONIC FORECASTING–WIND DFIG-PV MODEL

1) VOLTAGE HARMONICS

The actual versus forecast curves of Voltage Total Harmonic Distortion (THDV) for all forecasting models i.e., 3LCRNNL, 3LCRNNG, 3LCRNNGL and ANFIS with subtractive clustering are presented in Fig. 7. There are a total of three variables that have been forecasted. The major one is the THDV followed by the individual harmonics 11th (h11) and 13th (h13) that are the dominant harmonics for voltage waveform. Fig. 8 and Fig. 9 presents the forecasting results for h11 and h13 respectively. To further analyze the error profile and accuracy of these models refer to Table 1 presenting the metrics calculated (RMSE and MAE).

From Table 2 it can be observed that ANFIS produces the best results with lowest RMSE (8.844%) and MAE (5.498%). As for the three ANN networks, it can be observed that 3LCRNNG performs better than the other two models producing RMSE and MAE of 9.098% and 5.547%. The

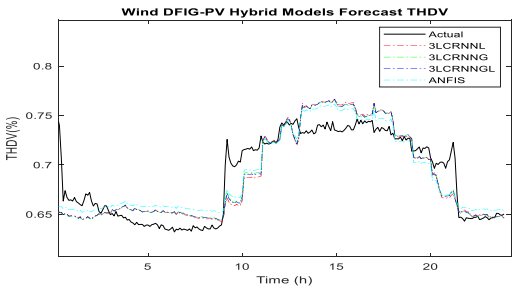

FIGURE 7. THDV – actual vs forecast curves Wind DFIG-PV model.

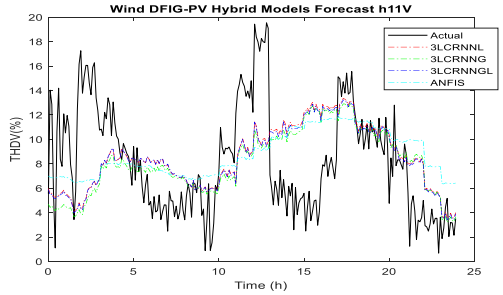

FIGURE 8. 11th harmonic voltage – Actual vs Forecast curves Wind DFIG-PV model.

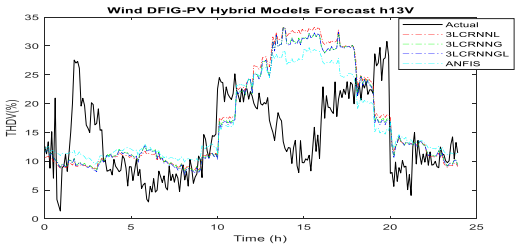

FIGURE 9. 13th harmonic voltage – Actual vs Forecast curves Wind DFIG-PV model.

TABLE 1. THDV forecast error profile for wind DFIG-PV model.

	RMSE (%)	MAE (%)
3LCRNNL	9.296%	5.680%
3LCRNNG	9.098%	5.547%
3LCRNNGL	9.138%	5.550%
ANFIS	8.844%	5.498%

TABLE 2. Voltage 11th harmonic forecast error for wind DFIG-PV model.

	RMSE (%)	MAE (%)
3LCRNNL	11.398%	9.035%
3LCRNNG	11.588%	9.142%
3LCRNNGL	11.335%	8.975%
ANFIS	11.392%	9.437%

TABLE 3. Voltage 13th harmonic forecast error for wind DFIG-PV model.

	RMSE (%)	MAE (%)
3LCRNNL	14.356%	10.437%
LCRNNG	13.776%	10.104%
3LCRNNGL	13.775%	10.097%
ANFIS	12.398%	9.526%

performances of proposed forecasting models for predicting the dominant individual voltage harmonics h11 and h13 are presented in Table 2 and 3.

Tables 2 and 3 suggest for h11, 3LCRNNGL performs best with lowest RMSE 11.335% and MAE 8.975%. For h13, ANFIS produces most accurate results with lowest RMSE

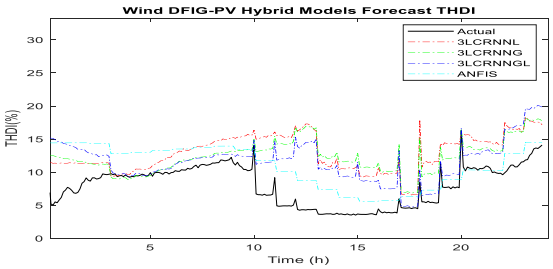

FIGURE 10. THDI – Actual vs Forecast curves Wind DFIG-PV model.

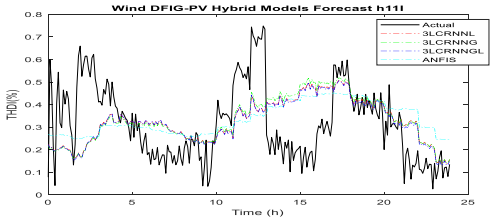

FIGURE 11. 11th harmonic current – Actual vs Forecast curves Wind DFIG-PV model.

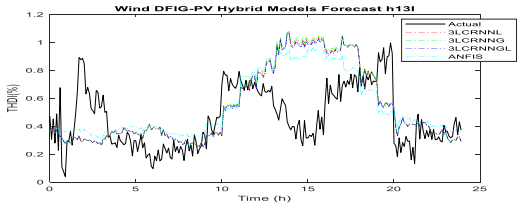

FIGURE 12. 13th harmonic current – Actual vs Forecast curves Wind DFIG-PV model.

TABLE 4. THDI forecast error for wind DFIG-PV model.

	RMSE (%)	MAE (%)
3LCRNNL	0.441%	0.350%
3LCRNNG	0.478%	0.378%
3LCRNNGL	0.378%	0.266%
ANFIS	0.668%	0.348%

and MAE of 12.398% and 9.526% respectively. An observation regarding three ANN models can be highlighted by comparing the results for three ANN networks. 3LCRNNGL tends to improve results as compared to the other two ANN models for h11 and h13 producing lowest RMSE and MAE.

ANFIS proves to be the best performing model for Wind DFIG-PV generator voltage total harmonic distortion and 13th harmonic, while 3LCRNNGL produces best forecast for 11th harmonic. Furthermore, it is observed that the improvement of 3LCRNNGL with all inputs cascaded to each layer and feedback both local and global tends to improve the performance of ANN as compared to the other proposed ANN models.

TABLE 5. Current 11th harmonic forecast error for wind DFIG-PV model.

	RMSE (%)	MAE (%)
3LCRNNL	11.434%	9.124%
3LCRNNG	11.624%	9.226%
3LCRNNGL	11.378%	9.047%
ANFIS	11.512%	9.567%

TABLE 6. Current 13 th harmonic forecast error for wind DFIG-PV model.

	RMSE (%)	MAE (%)
3LCRNNL	13.166%	9.614%
3LCRNNG	13.425%	9.777%
3LCRNNGL	13.041%	9.554%
ANFIS	12.042%	9.266%

2) CURRENT HARMONICS

This section presents the actual versus forecasted curves for the forecasting models used to predict the Current Total Harmonic Distortion, 11th and 13th harmonics for current waveform. Fig. 9, Fig. 10 & Fig. 11 presents the THDI, h11 and h13 harmonics actual vs forecast curves, while Tables 4, 5 and 6 summarizing the performance of each model.

For THDI and h11, 3LCRNNGL outperforms all the other predicting models with lowest RMSE% of 0.378% and 11.378% respectively. Whereas, for h13, ANFIS leads the results with 12.042% RMSE. Also, for three ANN models, 3LCRNNGL produces the better results than 3LCRNNL and 3LCRNNG.

B. HARMONIC FORECASTING—WIND PMSG-PV MODEL

1) VOLTAGE HARMONICS

The actual versus predicted curves for all proposed models for wind PMSG-PV generator model is presented in Fig. 13, Fig. 14 & Fig. 15 for THDV, h11 and h13 harmonics. Tables 7, 8 and 9 shows the error profile for VTHD, 11th and 13th voltage harmonics (h11 & h13).

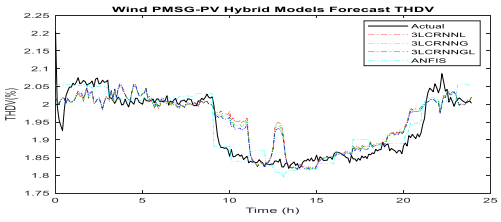

FIGURE 13. THDV – Actual vs forecast curves Wind PMSG-PV model.

Looking at Table 7, the overall performance of all models has shown accurate predictions with percent RMSE for all models below 6% and MAE percentage below 5%, each model has predicted quite accurately. To single out the best performing model, ANFIS employing subtractive clustering has proved to be the best in terms of all error performance matrices with RMSE of 3.969% and MAE 2.8%.

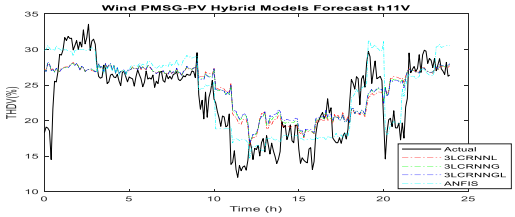

FIGURE 14. 11th harmonic current – Actual vs Forecast curves Wind PMSG-PV model.

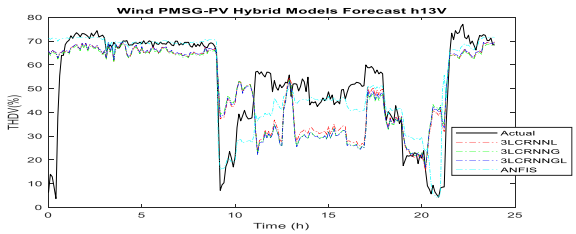

FIGURE 15. 13th harmonic current – Actual vs Forecast curves Wind PMSG-PV model.

TABLE 7. THDV forecast error for wind DFIG-PV model.

	RMSE (%)	MAE (%)
3LCRNNL	5.913%	4.295%
3LCRNNG	5.583%	4.100%
3LCRNNGL	5.289%	3.900%
ANFIS	3.969%	2.800%

TABLE 8. Voltage 11th harmonic forecast error for wind PMSG-PV model.

	RMSE (%)	MAE (%)
3LCRNNL	11.386%	8.830%
3LCRNNG	11.351%	8.807%
3LCRNNGL	11.414%	8.881%
ANFIS	10.303%	6.823%

TABLE 9. Voltage 13th harmonic forecast error for wind PMSG-PV model.

	RMSE (%)	MAE (%)
3LCRNNL	19.245%	13.477%
3LCRNNG	20.206%	14.492%
3LCRNNGL	20.042%	14.094%
ANFIS	14.709%	7.680%

Results for h11 and h13 voltage waveform indicates that with ANFIS has the lowest RMSE of 10.303% and 14.709% respectively as depicted in Tables 8 and 9. For ANN based models, CRNNGL performed better for THDV while, 3LCRNNG with 11.351% and 3LCRNNL with 19.245% RMSE have performed better for h11 and h13 respectively.

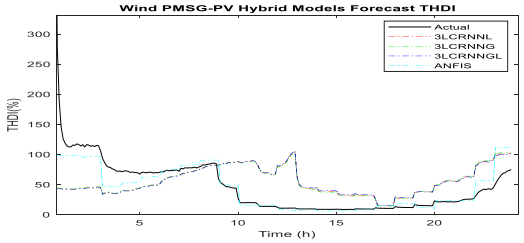

FIGURE 16. THDI – Actual vs Forecast curves Wind PMSG-PV model.

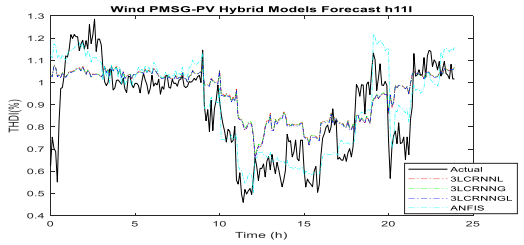

FIGURE 17. 11^{th} harmonic current – Actual vs Forecast curves Wind PMSG-PV model.

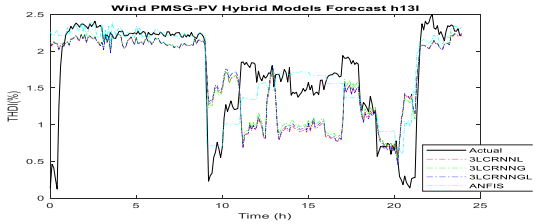

FIGURE 18. 13^{th} harmonic current – Actual vs Forecast curves Wind PMSG-PV model.

TABLE 10. THDI forecast error for wind PMSG-PV model.

	RMSE (%)	MAE (%)
3LCRNNL	7.155%	1.686%
3LCRNNG	7.147%	1.666%
3LCRNNGL	7.151%	1.671%
ANFIS	6.921%	0.946%

TABLE 11. Current 11^{th} harmonic forecast error for wind PMSG-PV model.

	RMSE (%)	MAE (%)
3LCRNNL	10.005%	7.824%
3LCRNNG	10.132%	7.938%
3LCRNNGL	10.140%	7.966%
ANFIS	7.652%	5.568%

2) CURRENT HARMONICS

The actual vs anticipated curves for the proposed forecasting models used to predict the THDI, 11^{th} and 13^{th} current harmonics for wind PMSG-PV model current harmonics is presented in Fig. 16, Fig. 17 & Fig. 18. The performance stats for forecasts for THDI, h11 and h13 for current waveform are presented in Tables 10, 11 & 12.

TABLE 12. Current 13^{th} harmonic forecast error for wind PMSG-PV model.

	RMSE (%)	MAE (%)
3LCRNNL	20.640%	14.771%
3LCRNNG	19.741%	13.942%
3LCRNNGL	20.694%	14.882%
ANFIS	15.082%	8.459%

TABLE 13. Best forecast for DFIG-PV model.

Case		Model	RMSE (%)	MAE (%)
Voltage	THDV	ANFIS	8.844%	5.498%
	h11	3LCRNNGL	11.335%	8.975%
	h13	ANFIS	12.298%	9.526%
Current	THDI	3LCRNNGL	0.378%	0.266%
	h11	3LCRNNGL	11.378%	9.047%
	h13	ANFIS	12.042%	9.266%

As per the results, ANFIS proves to be the best performing model for all cases. With lowest RMSE and MAE for THDI (6.921% & 0.946%), h11 (7.652% & 5.568%) and h13 (15.082% & 8.459%) ANFIS produce results with highest accuracy. Among the three ANN models, 3LCRNNG with 7.147% and 19.741% RMSE produces better results than other ANN models for THDI and h13. While for h11, 3LCRNNL performed best among ANN based models with 10.005% RMSE.

VIII. CONCLUSION

Two renewable hybrid generator models (Wind DFIG-PV and Wind PMSG-PV) were developed in order to take real world wind speed and solar irradiation data of Halifax as input and simulate the power generated with respective current and voltage waveforms. Harmonics were extracted from these waveforms and were used to organize, train and forecast the dataset. Three multi layered ANN network architectures were proposed using the hyperbolic tangent as transfer function and scaled conjugate gradient for optimizing and training. Furthermore, ANFIS method was also utilized with subtractive clustering technique for training. An analysis of the harmonics forecast results shows that ANFIS based forecasting model has proven to be better and more accurate in most cases. To conclude the results and best models' Tables 13 and 14 present the best performing models for both generators for voltage and current harmonic parameters.

For Wind DFIG-PV model voltage harmonics forecast, ANFIS recorded the best performance for THDV and h13 with 8.844% and 12.298% RMSE and 3LCRNNGL for h11 with 11.335% RMSE. For current harmonics 3LCRNNGL proved to be most accurate for THDI (0.378%) and h11 (11.378%) predictions, while ANFIS was the best for h13 (12.042%). The corresponding percent RMSE and MAE results for best performing models are presented in Table 13:

TABLE 14. Best forecast for PMSG-PV model.

Case		Model	RMSE (%)	MAE (%)
Voltage	THDV	ANFIS	3.939%	2.800%
	h11	ANFIS	10.303%	6.823%
	h13	ANFIS	14.709%	7.680%
Current	THDI	ANFIS	6.921%	0.946%
	h11	ANFIS	7.652%	5.568%
	h13	ANFIS	15.082%	8.459%

The forecasting performance of proposed prediction models for wind PMSG-PV is summarized in Table 14. ANFIS produces the best results, for all cases both for voltage and current harmonics. For voltage THDV, h11 and h13 had 3.939%, 10.303% and 14.709% RMSE respectively. While, for current THDI with 6.921%, h11 with 7.652% and h13 with 15.082% had the lowest RMSE as compared to the proposed ANN results.

In order to improve the results, a recommended way forward is to create a hybrid forecasting model to improve adaptability of the network and improve forecasting accuracy.

REFERENCES

[1] P. F. Keebler, "Meshing power quality and electromagnetic compatibility for tomorrow's smart grid," *IEEE Electromagn. Compat. Mag.*, vol. 1, no. 2, pp. 100–103, 2nd Quart., 2012.

[2] F. A. Hadi, H. H. H. Aly, and T. Little, "A proposed adaptive filter for harmonics mitigation based on adaptive neuro fuzzy inference system model for hybrid wind solar energy system," in *Proc. IEEE Can. Conf. Electr. Comput. Eng. (CCECE)*, Sep. 2022, pp. 165–169.

[3] G. M. Shafiullah and A. M. T. Oo, "Analysis of harmonics with renewable energy integration into the distribution network," in *Proc. IEEE Innov. Smart Grid Technol. Asia (ISGT ASIA)*, Nov. 2015, pp. 1–6, doi: 10.1109/ISGT-Asia.2015.7387191.

[4] F. Al Hadi, H. H. H. Aly, and T. Little, "Harmonics prediction and mitigation using adaptive neuro fuzzy inference system model based on hybrid of wind solar driven by DFIG," in *Proc. IEEE 13th Annu. Inf. Technol., Electron. Mobile Commun. Conf. (IEMCON)*, Oct. 2022, pp. 338–342.

[5] F. Alhaddad, H. H. Aly, and M. El-Hawary, "An overview of active power filters for harmonics mitigation of renewable energies resources," in *Proc. IEEE 10th Annu. Inf. Technol., Electron. Mobile Commun. Conf. (IEMCON)*, Oct. 2019, pp. 386–393.

[6] A. Cheng, "Pac-GAN: Packet generation of network traffic using generative adversarial networks," in *Proc. Annual Inf. Technol., Electron. Mobile Commun. Conf.*, Vancouver, BC, Canada, Jan. 2019, pp. 1–5.

[7] *Product Data Bulletin: Power System Harmonics Causes and Effects of Variable Frequency Drives Relative*, Standard 519–1992, Square D, Aug. 1994.

[8] *IEEE Recommended Practice and Requirements for Harmonic Control in Electric Power Systems*, Standard 519–2014, 2014, pp. 1–29.

[9] *Limits for Harmonics Current Emissions (Equipment in-Put Current< 16 A Per Phase)*, Standard IEC 61000-3-2, International Electrotechnical Commission, 2005.

[10] *Limitation of Emission of Harmonic Currents in Low-Voltage Power Supply System's Equipment With Rated Current Greater Than 16 A*, Standard IEC Std, 61000-3-4, 1998.

[11] *General Guide on Harmonics and Interharmonics Measurements and Instrumentation for Power Supply and Equipment Connected Thereto*, Standard IEC 61000-4-7, International Electrotechnical Commission, 2002.

[12] S. K. Jain and S. N. Singh, "Harmonics estimation in emerging power system: Key issues and challenges," *Electr. Power Syst. Res.*, vol. 81, no. 9, pp. 1754–1766, Sep. 2011.

[13] T. Ortmeyer and K. Chakravarthi, "The effects of power system harmonics on power system equipment and loads," *IEEE Trans. Power App. Syst.*, vol. PAS-104, no. 9, pp. 2555–2563, Jan. 1985.

[14] V. E. Wagner, "Effects of harmonics on equipment," *IEEE Trans. Power Del.*, vol. 8, no. 2, pp. 672–680, Apr. 1993.

[15] A. B. Nassif, W. Xu, and W. Freitas, "An investigation on the selection of filter topologies for passive filter applications," *IEEE Trans. Power Del.*, vol. 24, no. 3, pp. 1710–1718, Jul. 2009.

[16] D. Bohaichuk, C. Muskens, and W. Xu, "Mitigation of harmonics in oil field electric systems using a centralized medium voltage filter," in *Proc. 9th Int. Conf. Harmon. Quality Power.*, Oct. 2000, pp. 614–618.

[17] C.-J. Chou, C.-W. Liu, J.-Y. Lee, and K.-D. Lee, "Optimal planning of large passive-harmonic-filters set at high voltage level," *IEEE Trans. Power Syst.*, vol. 15, no. 1, pp. 433–441, Feb. 2000.

[18] A. S. Yilmaz, A. Alkan, and M. H. Asyali, "Applications of parametric spectral estimation methods on detection of power system harmonics," *Electr. Power Syst. Res.*, vol. 78, no. 4, pp. 683–693, Apr. 2008.

[19] A. Yazdani and R. Iravani, *Voltage-Sourced Converters in Power Systems: Modeling, Control, and Applications*. Hoboken, NJ, USA: Wiley, 2010.

[20] N. Mohan, T. M. Undeland, and W. P. Robbins, *Power Electronics: Converters, Applications, and Design*. Hoboken, NJ, USA: Wiley, 2003.

[21] P. K. Ray, P. S. Puhan, and G. Panda, "Real time harmonics estimation of distorted power system signal," *Int. J. Electr. Power Energy Syst.*, vol. 75, pp. 91–98, Feb. 2016.

[22] P. M. Ivry, O. A. Oke, D. W. P. Thomas, and M. Sumner, "Predicting harmonic distortion of multiple converters in a power system," *J. Electr. Comput. Eng.*, vol. 2017, pp. 1–10, Jun. 2017.

[23] M. M. H. Alhaj, N. M. Nor, V. S. Asirvadam, and M. F. Abdullah, "Comparison of power system harmonic prediction," *Proc. Technol.*, vol. 11, pp. 628–634, Jan. 2013.

[24] M. Panoiu, C. Panoiu, and L. Ghiormez, "Neuro-fuzzy modeling and prediction of current total harmonic distortion for high power nonlinear loads," in *Proc. Innov. Intell. Syst. Appl. (INISTA)*, Jul. 2018, pp. 1–7.

[25] P. Rodríguez-Pajarón, A. H. Bayo, and J. V. Milanović, "Forecasting voltage harmonic distortion in residential distribution networks using smart meter data," *Int. J. Electr. Power Energy Syst.*, vol. 136, Mar. 2022, Art. no. 107653.

[26] H. Mori and S. Suga, "Power system harmonics prediction with an artificial neural network," in *Proc. IEEE Int. Sympoisum Circuits Syst.*, Jun. 1991, pp. 1129–1132.

[27] E. M. Kuyunani, A. N. Hasan, and T. Shongwe, "Improving voltage harmonics forecasting at a wind farm using deep learning techniques," in *Proc. IEEE 30th Int. Symp. Ind. Electron. (ISIE)*, Jun. 2021, pp. 1–6.

[28] M. Žnidarec, Z. Klaić, D. Šljivac, and B. Dumnić, "Harmonic distortion prediction model of a grid-tie photovoltaic inverter using an artificial neural network," *Energies*, vol. 12, no. 5, p. 790, Feb. 2019.

[29] A. Y. Hatata and M. Eladawy, "Prediction of the true harmonic current contribution of nonlinear loads using NARX neural network," *Alexandria Eng. J.*, vol. 57, no. 3, pp. 1509–1518, Sep. 2018.

[30] W. XiangJun and M. M. Y. Al-Hashimi, "The comparison of adaptive neuro-fuzzy inference system (ANFIS) with nonlinear regression for estimation and prediction," in *Proc. Int. Conf. Inf. Technol. e-Services*, Mar. 2012, pp. 1–7.

[31] H. H. H. Aly, "A proposed intelligent short-term load forecasting hybrid models of ANN, WNN and KF based on clustering techniques for smart grid," *Electr. Power Syst. Res.*, vol. 182, May 2020, Art. no. 106191.

[32] *Wind Farm DFIG Detailed Model*, MATLAB & Simulink, Bangalore, India, Sep. 2022.

[33] H. B. Demuth and M. H. Beale, *DATASET Typical Meteorological Data Access Service*, 7th ed. MathWorks, 2000.

[34] *MODEL Detailed Modelling of a 1.5mw Wind Turbine Based on Direct-Driven PMSG*, Jan. 2020.

[35] W. S. McCulloch and W. Pitts, "A logical calculus of ideas immanent in nervous activity," *Bull. Math. Biophys.*, vol. 5, no. 4, pp. 115–133, Dec. 1943.

[36] H. Demuth and M. Beale, "Neural network toolbox for use with MATLAB," DATASET Typical Meteorol. Data, Nat. Renew. Energy Lab. (NREL), USA, Tech. Rep., Apr. 2022, vol. 9. [Online]. Available: https://nsrdb.nrel.gov/data-sets/tmy

[37] M. F. Møller, "A scaled conjugate gradient algorithm for fast supervised learning," *Neural Netw.*, vol. 6, no. 4, pp. 525–533, Jan. 1993.
[38] H. H. H. Aly, "A novel deep learning intelligent clustered hybrid models for wind speed and power forecasting," *Energy*, vol. 213, Dec. 2020, Art. no. 118773.
[39] H. H. H. Aly, "A hybrid optimized model of adaptive neuro-fuzzy inference system, recurrent Kalman filter and neuro-wavelet for wind power forecasting driven by DFIG," *Energy*, vol. 239, Jan. 2022, Art. no. 122367.
[40] R. R. Yager and D. P. Filev, "Generation of fuzzy rules by mountain clustering," *J. Intell. Fuzzy Syst.*, vol. 2, no. 3, pp. 209–219, 1994.
[41] S. M. M. Alam and M. H. Ali, "A new subtractive clustering based ANFIS system for residential load forecasting," in *Proc. IEEE Power Energy Soc. Innov. Smart Grid Technol. Conf. (ISGT)*, Feb. 2020, pp. 1–5.

FAWAZ M. AL HADI received the B.Sc. degree in electrical engineering from the Riyadh College of Technology, Saudi Arabia, in 2007, and the M.Sc. degree from Dalhousie University, in 2014, where he is currently pursuing the Ph.D. degree in electrical and computer engineering. His research interest includes renewable energy integration.

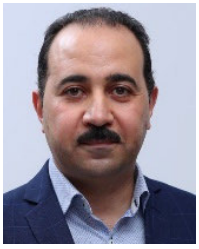

HAMED H. ALY (Senior Member, IEEE) received the B.Eng. and M.A.Sc. degrees (Hons.) in electrical engineering from Zagazig University, Egypt, in 1999 and 2005, respectively, and the Ph.D. degree from Dalhousie University, Canada, in 2012. He was a Postdoctoral Research Associate for one year and an Instructor for three years with Dalhousie University. He was with Acadia University as an Assistant Professor for three years. He is currently an Assistant Professor with Dalhousie University. His research interests include micro grids, smart grids, distributed generation, power quality issues, applications of artificial intelligence in power systems, energy management, green energy, and optimization.

TIMOTHY LITTLE is currently an Associate Dean of the Faculty of Engineering and a full-time Associate Professor with the Department of Electrical and Computer Engineering, Dalhousie University, Canada. His research interests include engineering education, wind energy and renewable generation, power electronics, and electromechanical energy conversion.